Pure & Appl. Chem., Vol. 57, No. 2, pp. 215–223, 1985.
Printed in Great Britain.

Magnetic Raman optical activity and Raman electron paramagnetic resonance

Laurence D. Barron

Chemistry Department, The University,
Glasgow, G12 8QQ, Scotland

Abstract - All molecules in a magnetic field parallel to the incident light beam show a small difference in the intensity of Raman scattering at 90° in right and left circularly polarized incident light. The most interesting effects occur in vibrational resonance Raman scattering from odd-electron transition metal halides, and in pure electronic resonance Raman scattering from both odd- and even-electron molecules. These effects originate in Raman transitions between components of Zeeman-split degenerate levels, and provide information about the magnetic structure of the ground and low-lying excited levels (in particular the sign of the g-value and the ordering of magnetic sub-states).

INTRODUCTION

All atoms and molecules in a magnetic field parallel to the incident light beam show optical rotation (the Faraday effect) and circular dichroism. These are examples of optical activity in transmitted light. Several years ago, Barron and Buckingham predicted that analogous optical activity effects should exist in scattered light (Ref. 1). Thus the intensity of Rayleigh and Raman light scattered at 90° from any atom or molecule in a magnetic field parallel to the incident light beam should be slightly different in right and left circularly polarized incident light. This circular intensity difference (CID) can be understood from the fact that all optical activity phenomena can be reduced to the common origin of a difference in response to right and left circularly polarized light (Ref. 2).

All the observations of magnetic Raman optical activity (ROA) to date have involved the resonance Raman effect in dilute solutions, effects in conventional transparent scattering being below current levels of detection. Magnetic ROA was first observed in a number of the vibrational bands in the resonance Raman spectrum of ferrocytochrome c (Ref. 3). More detailed studies of this sample revealed that the effects originate in the Zeeman splitting of the degenerate excited resonant level, and depend both on the symmetry species of the associated vibration and on the precise details of the resonance Raman process (Ref. 4). Magnetic ROA has also been observed in vibrational resonance Raman scattering from odd-electron transition metal halides (Ref. 5 & 6), and in pure electronic resonance Raman scattering from both odd- and even-electron molecules (Ref. 7). Only the latter effects, which are the most interesting, are described here: they originate in Raman transitions between the Zeeman-split components of degenerate levels. Reference 8 contains a detailed recent review of both types of magnetic ROA.

Antisymmetric scattering tensors can make important contributions to Rayleigh and Raman scattering at resonance, but vanish at transparent frequencies (Ref. 2, 9 & 10). Mainly because antisymmetric Raman scattering transitions are allowed between initial and final states that would normally be connected by a magnetic dipole operator, antisymmetric scattering plays a central rôle in many of the magnetic ROA effects that have been observed, and these effects can sometimes provide a more sensitive test for antisymmetric scattering than the depolarization ratio anomalies by which it is usually characterised. Atoms and molecules in degenerate states constitute an important source of antisymmetric scattering; and the magnetic ROA experiments add a new dimension to the studies of these systems and provide detailed information about the magnetic structure of ground and low-lying excited degenerate states, in particular the sign of the g-value and the ordering of magnetic sub-states in general. Thus magnetic ROA can function as Raman electron paramagnetic resonance (EPR).

Rayleigh and Raman optical activity was actually studied first in chiral molecules for which no magnetic field is necessary since they exhibit natural optical activity (Ref. 11). Natural ROA is now well-established as a means of measuring optical activity associated with vibrational transitions in chiral molecules, and has been shown to provide detailed stereochemical information. References 12, 13 & 14 contain recent reviews of natural vibrational

ROA, while 15 & 16 contain reviews that discuss this topic together with infrared circular dichroism from a unified standpoint as complementary techniques for measuring vibrational optical activity.

LIGHT SCATTERING IN A MAGNETIC FIELD

Our experimental quantity is the dimensionless CID

$$\Delta_\alpha = (I_\alpha^R - I_\alpha^L)/(I_\alpha^R + I_\alpha^L) \tag{1}$$

where I_α^R and I_α^L are the α-components of the scattered intensities in right and left circularly polarized incident light. Referring to Fig. 1, we can define polarized and depolarized CIDs Δ_x and Δz corresponding to intensity components I_x and I_z being measured through an analyzer with its transmission axis perpendicular and parallel to the scattering plane yz. We use

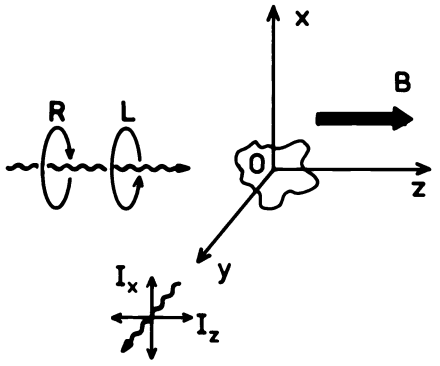

Fig. 1. The geometry for polarized light scattering in a magnetic field.

a semi-classical formulation in which scattered light originates in the characteristic radiation fields generated by the oscillating electric and magnetic multipole moments induced in a molecule by the incident light wave.

In cartesian tensor notation, the α-component of the electric dipole moment is defined as

$$\mu_\alpha = \sum_i e_i r_{i_\alpha} \tag{2}$$

where particle i at $\underset{\sim}{r}_i$ has charge e_i, mass m_i and momentum $\underset{\sim}{p}_i$. The corresponding magnetic dipole moment is

$$m_\alpha = \sum_i (e_i/2m_i)\epsilon_{\alpha\beta\gamma} r_{i_\beta} p_{i_\gamma} \tag{3}$$

where $\epsilon_{\alpha\beta\gamma}$ is the unit third rank antisymmetric tensor, a repeated Greek suffix denoting summation over the three components. The real oscillating electric dipole moment induced by the real electric vector $\underset{\sim}{E}$ of the light wave is written

$$\mu_\alpha = \alpha_{\alpha\beta} E_\beta + \frac{1}{\omega} \alpha'_{\alpha\beta} \dot{E}_\beta + - - - \tag{4}$$

where $\alpha_{\alpha\beta}$ and $\alpha'_{\alpha\beta}$ are the symmetric and antisymmetric polarizability tensors for which time-dependent perturbation theory gives the following expressions (Ref. 2):

$$\alpha_{\alpha\beta} = \frac{2}{\hbar} \sum_{j \neq n} \frac{\omega_{jn}}{\omega_{jn}^2 - \omega^2} \mathrm{Re}(\langle n|\mu_\alpha|j\rangle\langle j|\mu_\beta|n\rangle) = \alpha_{\beta\alpha} \tag{5a}$$

$$\alpha'_{\alpha\beta} = -\frac{2}{\hbar} \sum_{j \neq n} \frac{\omega}{\omega_{jn}^2 - \omega^2} \mathrm{Im}(\langle n|\mu_\alpha|j\rangle\langle j|\mu_\beta|n\rangle) = -\alpha'_{\beta\alpha} \tag{5b}$$

where ω is the angular frequency, $\omega_{jn} = \omega_j - \omega_n$, and $|n\rangle$ and $|j\rangle$ are the initial and intermediate states of the molecule. It is convenient to present these results in a complex representation. Introducing the complex polarizability tensor (a tilde denotes a complex quantity)

$$\tilde{\alpha}_{\alpha\beta} = \alpha_{\alpha\beta} - i\alpha'_{\alpha\beta} = \tilde{\alpha}^*_{\beta\alpha} \tag{6}$$

the amplitude of the complex oscillating electric dipole moment induced by the complex electric vector $\tilde{\underset{\sim}{E}}$ can be written

$$\tilde{\mu}^{(o)}_{\alpha} = \tilde{\alpha}_{\alpha\beta}\tilde{E}^{(o)}_{\beta} + - - - \tag{7}$$

By writing $\tilde{\underset{\sim}{E}}^{(\omega)}$ explicitly for right and left circularly polarized incident light and calculating the corresponding scattered intensities, the required circular intensity differences and sums are found to be (Ref. 1, 2 & 8)

$$I^R_x - I^L_x = \frac{\omega^2\mu_o E^{(o)2}}{16\pi^2 cy^2}\,\mathrm{Im}(\tilde{\alpha}_{xy}\tilde{\alpha}^*_{xx} + - - -) \tag{8a}$$

$$I^R_z - I^L_z = \frac{\omega^2\mu_o E^{(o)2}}{16\pi^2 cy^2}\,\mathrm{Im}(\tilde{\alpha}_{zy}\tilde{\alpha}^*_{zx} + - - -) \tag{8b}$$

$$I^R_x + I^L_x = \frac{\omega^4\mu_o E^{(o)2}}{32\pi^2 cy^2}\,(\tilde{\alpha}_{xx}\tilde{\alpha}^*_{xx} + \tilde{\alpha}_{xy}\tilde{\alpha}^*_{xy} + - - -) \tag{8c}$$

$$I^R_z + I^L_z = \frac{\omega^4\mu_o E^{(o)2}}{32\pi^2 cy^2}\,(\tilde{\alpha}_{zx}\tilde{\alpha}^*_{zx} + \tilde{\alpha}_{zy}\tilde{\alpha}^*_{zy} + - - -) \tag{8d}$$

where μ_o is the permeability of free space.

The results so far apply to Rayleigh scattering. For Raman scattering between initial and final states $|n\rangle$ and $|m\rangle$ we introduce a complex transition polarizability given by

$$(\tilde{\alpha}_{\alpha\beta})_{mn} = \frac{1}{\hbar}\sum_{j\neq n,m}\left[\frac{\langle m|\mu_\alpha|j\rangle\langle j|\mu_\beta|n\rangle}{\omega_{jn} - \omega} + \frac{\langle m|\mu_\beta|j\rangle\langle j|\mu_\alpha|n\rangle}{\omega_{jm} + \omega}\right] \tag{9}$$

By taking $|n\rangle = |m\rangle$ and separating real and imaginary parts, the polarizabilities (5a & b) are recovered. This complex transition polarizability can be generated as the general matrix element of the following effective polarizability operator (Ref. 2 & 10)

$$\hat{\alpha}_{\alpha\beta} = \hat{\alpha}^+_{\alpha\beta} + \hat{\alpha}^-_{\alpha\beta} \tag{10a}$$

$$\hat{\alpha}^{\pm}_{\alpha\beta} = \pm\tfrac{1}{2}(\mu_\alpha O^{\pm}\mu_\beta \pm \mu_\beta O^{\pm}\mu_\alpha) = \pm\hat{\alpha}^{\pm}_{\beta\alpha} \tag{10b}$$

$$O^{\pm} = \left(\frac{1}{H-\bar{W}+\hbar\omega} \pm \frac{1}{H-\bar{W}-\hbar\omega}\right) \tag{10c}$$

where $\bar{W}$ is the average of the energies W_n and W_m. By summing over a complete set of states $|j\rangle\langle j|$ inserted after $O^{\pm}$, and taking $\omega_{jn} \approx \omega_{jm}$, it is easily verified that $\langle m|\hat{\alpha}_{\alpha\beta}|n\rangle$ generates (9). The importance of this operator is that the separate parts $\hat{\alpha}^+_{\alpha\beta}$ and $\hat{\alpha}^-_{\alpha\beta}$ behave differently under time reversal, which is central to the symmetry classification of transition polarizabilities in degenerate systems. Time-even (+) and time-odd (-) operators are defined by

$$\Theta A(\pm)\Theta^{-1} = \pm A(\pm)^{\dagger} \tag{11}$$

where $A^{\dagger}$ is the Hermitian conjugate of A, and Θ is the time reversal operator that first takes the complex conjugate of a wavefunction and then reverses the sign of the time coordinate. It can be shown that $\hat{\alpha}^+_{\alpha\beta}$ is a time-even, Hermitian, even parity operator; whereas $\hat{\alpha}^-_{\alpha\beta}$ is a time-odd, anti-Hermitian, even parity operator. This enables the following fundamental property of the transition polarizability to be deduced (Ref. 2 & 10):

$$\langle m|\hat{\alpha}_{\alpha\beta}|n\rangle = \langle\Theta n|\hat{\alpha}_{\beta\alpha}|\Theta m\rangle = \langle\Theta m|\hat{\alpha}_{\alpha\beta}|\Theta n\rangle^* \tag{12}$$

For an even-electron system the initial and final states can always be chosen to be even with respect to time reversal, that is $|\hat{\Theta}n\rangle = |n\rangle$ and $|\hat{\Theta}m\rangle = |m\rangle$, so that

$$\langle m|\hat{\alpha}_{\alpha\beta}|n\rangle = \langle m|\hat{\alpha}_{\alpha\beta}|n\rangle^{*} \tag{13}$$

This shows that the transition polarizability is pure real, but says nothing about its permutation symmetry so that both symmetric and antisymmetric parts are allowed by time reversal. If m = n, however, it follows from the first equality in (12) that only the symmetric part survives so that antisymmetric Rayleigh scattering is forbidden. For an odd-electron system it is not possible to construct states that are even or odd with respect to time reversal. We consider a scattering transition involving a Kramers-conjugate pair of effective spin states $|+\tfrac{1}{2}\rangle$ and $|-\tfrac{1}{2}\rangle$ so that $\hat{\Theta}|+\tfrac{1}{2}\rangle = |-\tfrac{1}{2}\rangle$ and $\hat{\Theta}|-\tfrac{1}{2}\rangle = -|+\tfrac{1}{2}\rangle$. Four scattering transitions are possible: $|+\tfrac{1}{2}\rangle \rightarrow |+\tfrac{1}{2}\rangle$, $|-\tfrac{1}{2}\rangle \rightarrow |-\tfrac{1}{2}\rangle$, $|+\tfrac{1}{2}\rangle \rightarrow |-\tfrac{1}{2}\rangle$ and $|-\tfrac{1}{2}\rangle \rightarrow |+\tfrac{1}{2}\rangle$; the first pair we call 'diagonal', the second pair 'off-diagonal'. Then from (12)

$$\langle +\tfrac{1}{2}|\hat{\alpha}_{\alpha\beta}|+\tfrac{1}{2}\rangle = \langle -\tfrac{1}{2}|\hat{\alpha}_{\beta\alpha}|-\tfrac{1}{2}\rangle = \langle -\tfrac{1}{2}|\hat{\alpha}_{\alpha\beta}|-\tfrac{1}{2}\rangle^{*} \tag{14a}$$

$$\langle -\tfrac{1}{2}|\hat{\alpha}_{\alpha\beta}|+\tfrac{1}{2}\rangle = -\langle -\tfrac{1}{2}|\hat{\alpha}_{\beta\alpha}|+\tfrac{1}{2}\rangle = -\langle +\tfrac{1}{2}|\hat{\alpha}_{\alpha\beta}|-\tfrac{1}{2}\rangle^{*} \tag{14b}$$

We deduce from (14a) that diagonal transitions can generate a complex transition polarizability with a real symmetric and an imaginary antisymmetric part, and from (14b) that 'off-diagonal' transitions can generate an antisymmetric polarizability with both real and imaginary parts.

We now use the circular intensity differences and sums (8) to write the following expressions for the dimensionless CIDs in terms of space-fixed components of the complex transition polarizability (9) :

$$\Delta_x = \frac{2\mathrm{Im}\left[(\tilde{\alpha}_{xy})_{mn}(\tilde{\alpha}_{xx})_{mn}^{*}\right]}{(\tilde{\alpha}_{xx})_{mn}(\tilde{\alpha}_{xx})_{mn}^{*} + (\tilde{\alpha}_{xy})_{mn}(\tilde{\alpha}_{xy})_{mn}^{*}} \tag{15a}$$

$$\Delta_z = \frac{2\mathrm{Im}\left[(\tilde{\alpha}_{zy})_{mn}(\tilde{\alpha}_{zx})_{mn}^{*}\right]}{(\tilde{\alpha}_{zx})_{mn}(\tilde{\alpha}_{zx})_{mn}^{*} + (\tilde{\alpha}_{zy})_{mn}(\tilde{\alpha}_{zy})_{mn}^{*}} \tag{15b}$$

These CIDs can be developed in two distinct ways. (a) For magnetic Rayleigh and Raman optical activity associated with a non-degenerate electronic level or with diagonal scattering transitions between the components of a degenerate electronic level, the transition polarizabilities are written perturbed to first order in the static magnetic field B_z and a weighted Boltzmann average taken over all the orientations of the molecules in the fluid sample. The results, which are rather complicated and are not reproduced here, can be found in References 1, 2 & 8. (b) For off-diagonal scattering transitions, it is possible to obtain useful approximate results by working directly from the CIDs (15) without performing the weighted average, particularly in atoms and in molecules such as octahedral complexes where the three principle axes are equivalent. This is because the magnetic field lifts the electronic degeneracy so that pairs of off-diagonal Raman transitions can occur leading to pairs of Raman bands displaced on either side of the original frequency by an amount equivalent to the Zeeman splitting.

RAMAN EPR AND THE SIGN OF THE g-VALUE

Magnetic optical activity in off-diagonal Raman transitions between the Zeeman components of degenerate levels is particularly interesting because it depends on the g-value and so functions as Raman EPR. Fig. 2a shows a conventional vibrational Stokes resonance Raman process, while 2b and 2c show the polarization characteristics of the two distinct off-diagonal Raman processes for scattering at 90° that are generated if a two-fold Kramers degeneracy in the initial and final levels is lifted by a magnetic field parallel to an incident light beam along the z-direction. Each scattering pathway can be envisaged as the longditudinal and transverse Zeeman effects back-to-back: the incident circularly polarized photon generates a $\Delta M = \pm 1$ change in the molecule, and the 90°-scattered z-polarized photon a $\Delta M = 0$ change. Two depolarized Raman lines, shifted in frequency by the Zeeman splitting δ on either side of the vibrational Raman frequency ω_v, are thereby generated. This mechanism provides a magnetic ROA couplet in a totally symmetric Raman band, the absolute signs of the lower and higher frequency components being positive and negative, respectively, for the ordering of the initial and final magnetic sub-states shown in Fig. 2 (the signs are independent of the ordering in the intermediate resonant state). Because the molecule suffers a $\Delta M = \pm 1$ change overall, the corresponding transition tensor is pure antisymmetric since it must transform like an axial vector: this conclusion also follows immediately from (14b). A related feature is that a transition between spin states has been effected by a scattering operator that contains no spin operator, but simply two spatial electric dipole

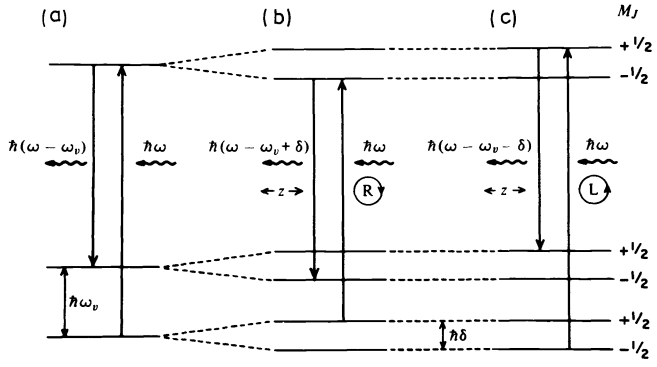

Fig. 2. Off-diagonal Raman scattering pathways.

moment operators. This implies that the intermediate resonant state must be a resolved spin-orbit state in which spin and orbital components are intimately mixed by the spin-orbit coupling operator, thereby providing a scattering pathway connecting different initial and final spin states.

In the Rayleigh case, the ground-state g-value could be measured as half the separation of the two lines displaced on either side of the central Rayleigh line, although this would require a sufficiently large magnetic field to resolve the lines (for a g-value of 2, a field of 1.07T produces a splitting of 1 cm^{-1}). Similarly for the Raman case, except that now the separation of the two bands on either side of the original Raman band is half the sum of the g-values for the ground level and the first excited vibrational level.

An additional feature is that the sign of the g-value is provided automatically, even if the resolution is insufficient to give the magnitude. The g-value is always positive in atoms and is usually assumed to be positive in molecules. In an isolated Kramers doublet, for example, this corresponds to the $S_z = -½$ state lying below the $S_z = +½$ state where S is the effective spin angular momentum. Occasionally, however, this order is reversed, being interpreted as a negative value of g, in which case the absolute signs of the lower and higher frequency components of the magnetic ROA couplet would be positive and negative, respectively, the opposite of that deduced from Fig. 2. The conventional method for determining the sign of g uses circularly polarized microwave radiation in an EPR experiment, but such experiments are rarely performed. Negative g-values have been discussed in detail by Abragam and Bleaney (Ref. 17), who indicate that the isotropic g-value of $IrCl_6^{2-}$ should be negative on theoretical grounds (see also Ref. 18). As discussed below, this has been confirmed from magnetic ROA observations.

EXPERIMENTAL

Our experimental arrangement in Glasgow, described in detail elsewhere (Ref. 8), is based on a modified scanning Raman spectrometer (Fig. 3). The sample is placed between the poles of

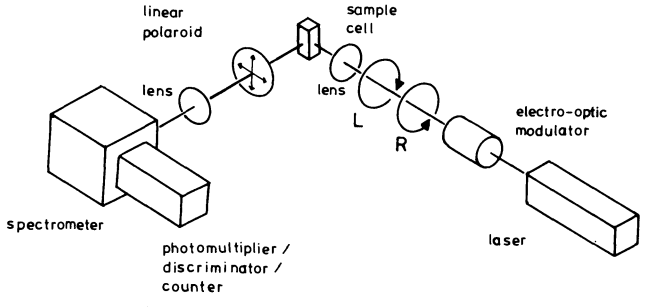

Fig. 3. Basic layout of the scanning Raman CID spectrometer.

an electromagnet with holes bored through the pole pieces so that the incident laser beam can be applied parallel to the magnetic field. An electro-optic modulator is used to switch the laser beam between right and left circular, the Raman circular intensity difference and

sum being extracted using dual synchronous photon counting. Using a small electromagnet that generates a field of 1.1T over a pole gap of 0.6 cm, well-defined $I^R - I^L$ spectra with an effective resolution of 10 - 15 cm^{-1} can be recorded at a scan rate of 1 cm^{-1} min^{-1} using 1W of argon-ion or dye laser power. Considerable improvement would be possible using an optical multichannel Raman instrument, which has been used with great effect for measuring natural ROA (Ref. 13).

We present raw photon count spectra of $I_\alpha^R + I_\alpha^L$ and $I_\alpha^R - I_\alpha^L$ separately because the background must be subtracted from $I_\alpha^R + I_\alpha^L$ before calculating the dimensionless CID Δ_α. Further, the $I_\alpha^R + I_\alpha^L$ spectra are presented on a linear scale, whereas the $I_\alpha^R - I_\alpha^L$ spectra are presented on a scale that is linear within each decade range but logarithmic between ranges: this enables the exponent in the $I_\alpha^R - I_\alpha^L$ photon count to be recorded, and shows up significant features on weak Raman bands that would be lost in the baseline of a conventional display.

Since all the magnetic ROA effects observed so far have involved resonance Raman scattering from dilute solutions of absorbing molecules, special precautions have been necessary to prevent decomposition. If sufficient material is available, we have found the best arrangement to be a small fluorescence cell situated between the poles of the magnet and connected to tubing at each end so that the sample solution can be flowed rapidly through by means of a peristaltic pump, with a large reservoir cooled in ice.

Magnetic ROA has been relatively free of the artefacts that have plagued natural ROA measurements. As discussed in detail elsewhere (Ref. 19), this might be due in part to the significant antisymmetric contributions that are often present.

TYPICAL MAGNETIC ROA SPECTRA

Magnetic vibrational ROA in odd-electron complexes

Fig. 4a shows the depolarized magnetic ROA spectrum of the high-spin d^5 complex $FeBr_4^-$ (Ref. 5). The two Raman bands are assigned to two of the four Raman-active fundamentals of the MX_4 structure, namely $\nu_1(A_1, 201\ cm^{-1})$ and $\nu_3(T_2, 290\ cm^{-1})$. A large CID couplet appears in the A_1 band, but none in the T_2 band. Since the sign of the couplet component

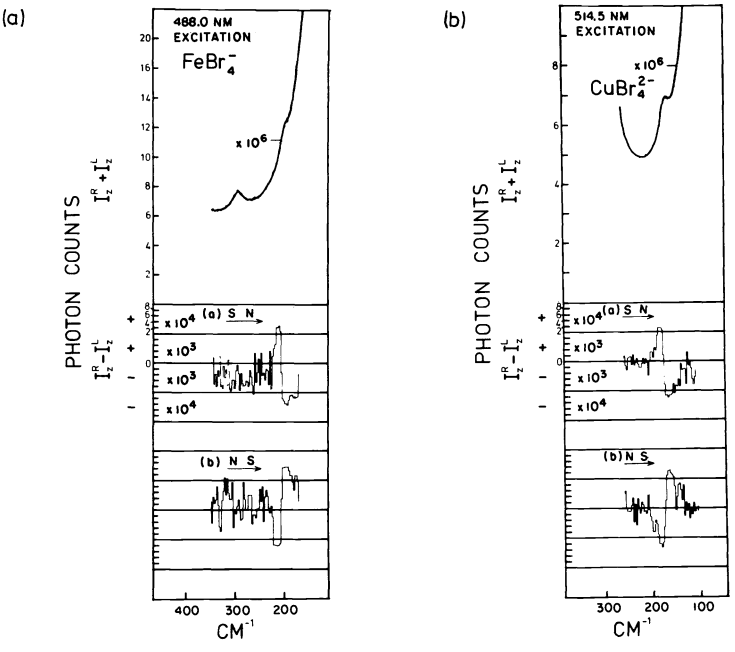

Fig. 4. The depolarized magnetic Raman circular intensity sum and difference spectra of (a) $FeBr_4^-$ in nitromethane and (b) $CuBr_4^{2-}$ in methylene dichloride. Field strength 0.7T.

having the lower Stokes Raman shift is positive in the positive magnetic field (N→S), we deduce from the earlier discussion that the g-value is positive.

Only one resonance Raman band was observed in the d^9 complex $CuBr_4^{2-}$, at about 174 cm^{-1}

(Fig. 4b), being assigned to the symmetric stretch $\nu_1(A_1)$. The appearance of the CID couplet was taken as unequivocal evidence for antisymmetric scattering, which had not previously been identified in this species: this was subsequently confirmed using complete polarization measurements (Ref. 20). Again the g-value is seen to be positive.

The low-spin d^5 complexes $IrCl_6^{2-}$ and $IrBr_6^{2-}$ have been studied in rather more detail, especially with regard to the influence of the excited resonant state on the appearance of the resonance Raman bands and the magnetic ROA. Fig. 5 shows the depolarized Stokes and anti-Stokes magnetic ROA spectrum of $IrCl_6^{2-}$ (Ref. 21). The three Raman-active fundamentals of the octahedral MX_6 structure are assigned to $\nu_1(A_{1g}, 341\ cm^{-1})$, $\nu_2(E_g, 290\ cm^{-1})$ and $\nu_5(T_{2g}, 161\ cm^{-1})$. The ground electronic level belongs to the $E_g''(^2T_{2g})$ Kramers doublet of O_h^*, and the excited resonant level to $U_u'(^2T_{1u}^{(1)})$ when 488.0nm excitation is used. The

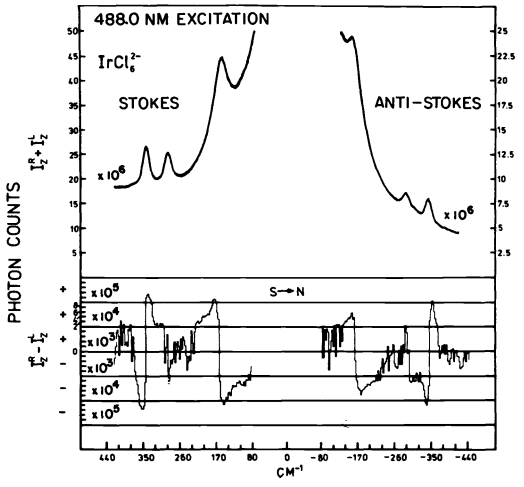

Fig. 5. Depolarized Stokes and anti-Stokes magnetic circular intensity sum and difference spectra of $IrCl_6^{2-}$ in dilute aqueous $HClO_4$ solution. Field strength 1.2T.

sharp couplet in the A_{1g} band at 341 cm^{-1} originates in the mechanism of Fig. 2, and since the magnetic field direction is negative (S→N), it follows directly from the fact that the lower Stokes frequency component is positive that the ground state g- factor is negative (Ref. 22). The explanation of the absolute signs observed in the E_g and T_{2g} couplets (the E_g couplet is more pronounced in $IrBr_6^{2-}$ using 514.5 nm excitation, Ref. 23) still remains obscure.

Magnetic electronic ROA

Magnetic optical activity in pure electronic resonance Raman transitions in solution samples of $OsBr_6^{2-}$, $IrCl_6^{2-}$ and uranocene have recently been reported (Ref. 7). All the features are associated with antisymmetric scattering because they all involve the molecule in a $\Delta M_J = \pm 1$ scattering transition. But because the electronic Raman transitions are between component states of different levels, the effects do not necessarily originate exclusively in antisymmetric scattering. Recall that the general selection rules for Raman transitions between magnetic quantum states are as follows (Ref. 9). Isotropic (trace) scattering: $\Delta J = 0$, $\Delta M = 0$. Traceless symmetric scattering: $\Delta J = 0, \pm1, \pm2$; $\Delta M = 0, \pm1, \pm2$; but not for $J = 0 \rightarrow 0$, $0 \rightarrow 1$, $1 \rightarrow 0$, $\frac{1}{2} \rightarrow \frac{1}{2}$. Antisymmetric scattering: $\Delta J = 0, \pm1$; $\Delta M = 0, \pm1$; but not for $J = 0 \rightarrow 0$. The observed effects have provided information about the signs of the g-values of the initial and final electronic Raman levels, and have confirmed in detail earlier assignments of the corresponding electronic transitions. Uranocene is particularly interesting in this respect and is now described in some detail.

Uranocene, $U(C_8H_8)_2$, has a D_{8h} structure with a U^{IV} ion sandwiched between two cyclo-octatetraenyl dianions. Laser excitation within the charge-transfer visible absorption bands between 600 and 700 nm produces a resonance Raman spectrum containing an anomalously polarized band at 466 cm^{-1} assigned to an electronic transition involving non-bonding 5f orbitals (Ref. 24). Using a simplified treatment based on the f^2 configuration in an effectively axial crystal field, the $^3H_4$ ground term splits into five levels corresponding to $M_J = 0, \pm1, \pm2, \pm3, \pm4$. Thus any Raman transitions within this set of levels is associated with $\Delta J = 0$, so both symmetric and antisymmetric contributions are possible, the former being associated with $\Delta M_J = 0, \pm1, \pm2$ and the latter with $\Delta M_J = 0, \pm1$, although time reversal arguments exclude $\Delta M_J = 0$ in the latter since J is integral (Ref. 2 & 10). Thus the antisymmetric Raman scattering in the 466 cm^{-1} band is associated exclusively with

$\Delta M_J = \pm 1$ transitions, which led to a re-interpretation of the magnetic susceptibility data from which it was concluded that the ground and first excited levels of uranocene are the $M_J = \pm 4$ and ± 3 components, respectively, of the $^3H_4$ manifold (Ref. 24). Dye laser excitation within the x,y-polarized absorption band at 641 nm produces an enormous magnetic ROA couplet in the 466 cm^{-1} electronic Raman band (Fig. 6a) which can be understood in terms

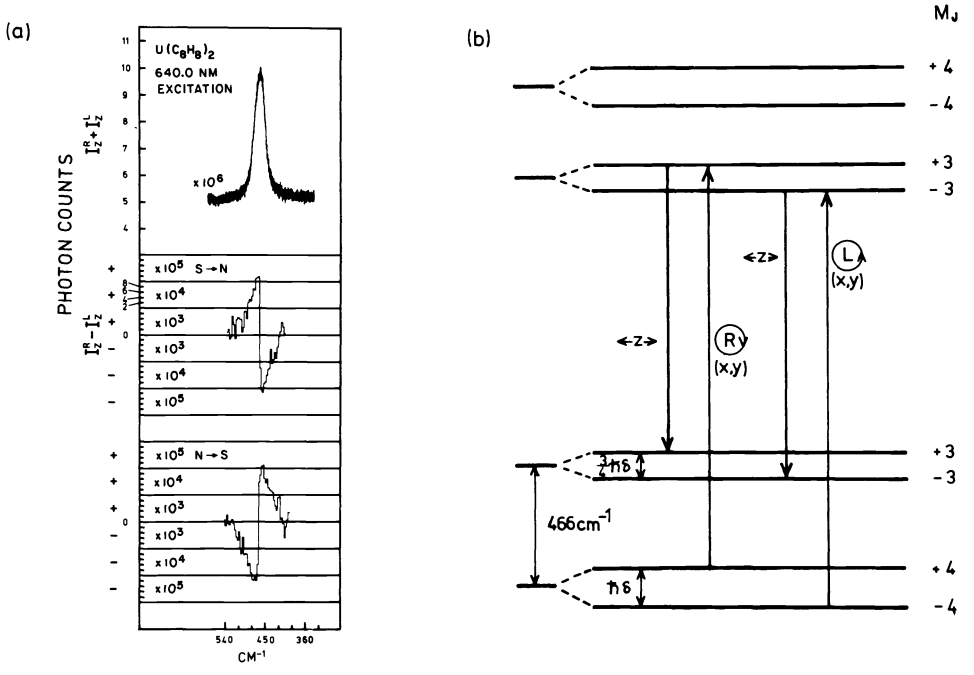

Fig. 6 (a) The depolarized magnetic circular intensity sum and difference spectra of the 466 cm^{-1} electronic Raman band of uranocene in tetrahydrofuran; field strength 1.2 T. (b) Electronic Raman pathways for the $M_J = \pm 3 \leftrightarrow M_J = \pm 4$ transitions in uranocene.

of the magnetic components of the $M_J = \pm 3 \leftrightarrow M_J = \pm 4$ transition (Fig. 6b). Since the absorption band is x,y-polarized, the transition to the excited resonant state must involve $\Delta M_J = \pm 1$. Assuming the g-factors of the $M_J = \pm 4$ and ± 3 levels are the same and positive, the Zeeman splitting of the ± 3 level will be ¾ that of the ± 4 level, so for a positive magnetic field (N → S) the lower frequency component of the magnetic ROA couplet should be positive and the higher frequency component negative. The fact that this is what is observed provides unequivocal evidence that the $|M_J|$ value of the ground level is greater by a factor of one than that of the first excited level, thus supporting the earlier deduction that the $M_J = \pm 4$ level lies lowest.

Uranocene also shows a very weak resonance Raman ban at 675 cm^{-1}. Excitation within the 641 nm absorption band generates a weak magnetic ROA couplet with the same sign as the 466 cm^{-1} band, which enabled the 675 cm^{-1} band to be assigned to a combination of the 466 cm^{-1} electronic transition with a totally symmetric vibrational transition at 211 cm^{-1}.

COMPARISON WITH THE RAMAN-ZEEMAN EFFECT

There have been several interesting studies reported recently by Ramdas et al. involving Raman scattering of circularly polarized light from magnetic excitations in dilute magnetic semiconductors in a magnetic field parallel to the incident light beam. For example, using a field of 6T, well-resolved depolarized Stokes and anti-Stokes magnon Raman bands are seen at 5.62 cm^{-1} resulting from spin-flip transitions of Mn^{2+} 3d electrons in $Cd_{0.6}Mn_{0.4}Te$ (Ref. 25). The Stokes band corresponds to $\Delta M_S = +1$ and only appears in left circularly polarized incident light, whereas the anti-Stokes band corresponds to $\Delta M_S = -1$ and only appears in right. This clearly corresponds to a magnetic ROA experiment where the Zeeman components are resolved. Furthermore, the mechanism suggested for these Raman-Zeeman transitions is one due to Fleury and Loudon (Ref. 26) for the scattering of light by magnons in crystals which relies on pure electric dipole transitions with resolved spin-orbit intermediate states. This parallels the requirement, discussed above, for magnetic ROA in $\Delta M_S = \pm 1$ transitions in Kramers doublets to involve well-resolved spin-orbit intermediate resonant states.

Acknowledgements - I wish to thank Dr. J. Vrbancich for valuable contributions to this work, and the Science and Engineering Research Council for financial support.

REFERENCES

1. L.D. Barron and A.D. Buckingham, Mol. Phys. 23, 145 (1972).
2. L.D. Barron, Molecular Light Scattering and Optical Activity, Cambridge University Press, Cambridge (1982).
3. L.D. Barron, Nature 257, 372 (1975).
4. L.D. Barron, C. Meehan and J. Vrbancich, J. Raman Spectrosc. 12, 251 (1982).
5. L.D. Barron and C. Meehan, Chem. Phys. Lett. 66, 44 (1979).
6. L.D. Barron, J. Vrbancich and R.S. Watts, Chem. Phys. Lett. 89, 71 (1982).
7. L.D. Barron and J. Vrbancich, J. Raman Spectrosc. 14, 118 (1983).
8. L.D. Barron and J. Vrbancich, in Advances in Infrared and Raman Spectroscopy, Vol. 12 (R.J.H. Clark and R.E. Hester, eds.), Heyden, London, in the press.
9. G. Placzek, in Handbuch der Radiologie, Vol. 6, part 2 (E. Marx, ed.), Akademische Verlagsgesellschaft, Berlin, p. 205 (1934).
10. L.D. Barron and E. Nørby Svendsen, in Advances in Infrared and Raman Spectroscopy, Vol. 8 (R.J.H. Clark and R.E. Hester, eds.), Heyden, London, p. 322 (1981).
11. L.D. Barron and A.D. Buckingham, Mol. Phys. 20, 1111 (1971).
12. L.D. Barron, in Optical Activity and Chiral Discrimination, (S.F. Mason, ed.), Reidel, Dordrecht, p.219 (1979).
13. W. Hug, in Raman Spectroscopy (J. Lascombe and P.V. Huong, eds.), Chichester, Wiley, p.3 (1982).
14. L.D. Barron and J. Vrbancich, Topics in Current Chemistry, 123, 151 (1984).
15. L.A. Nafie, in Vibrational Spectra and Structure, Vol. 10 (J.R. Durig, ed.), Elsevier, Amsterdam, p. 153 (1981).
16. L.A. Nafie, in Advances in Infrared and Raman Spectroscopy, Vol. 11 (R.J.H. Clark and R.E. Hester, eds.), Heyden, London, p. 49 (1984).
17. A. Abragam and B. Bleaney, Electron Paramagnetic Resonance of Transition Ions, Clarendon Press, Oxford (1970).
18. P.N. Schatz, Mol. Phys. 47, 673 (1982).
19. L.D. Barron and J. Vrbancich, J. Raman Spectrosc. 15, 47 (1984).
20. P. Stein, P.W. Jensen and T.G. Spiro, Chem. Phys. Lett. 80, 451 (1981).
21. L.D. Barron and J. Vrbancich, Chem. Phys. Lett. 92, 466 (1982).
22. L.D. Barron, C. Meehan and J. Vrbancich, Mol. Phys. 41, 945 (1980).
23. L.D. Barron, J. Vrbancich and R.S. Watts, Chem. Phys. Lett. 89, 71 (1982).
24. R.F. Dallinger, P. Stein and T.G. Spiro, J. Am. Chem. Soc. 100, 7865 (1978).
25. A. Petrou, D.L. Peterson, S. Venugopalan, R.R. Galazka, A.K. Ramdas and S. Rodriguez, Phys. Rev. Lett. 48, 1036 (1982).
26. P.A. Fleury and R. Loudon, Phys. Rev. 166, 514 (1968).